JGR Biogeosciences

RESEARCH ARTICLE
10.1029/2018JG004684

Modeling Benthic Versus Hyporheic Nutrient Uptake in Unshaded Streams With Varying Substrates

Kevin R. Roche[1], Arial J. Shogren[2], Antoine Aubeneau[3], Jennifer L. Tank[2], and Diogo Bolster[1]

[1]Department of Civil & Environmental Engineering & Earth Sciences, University of Notre Dame, Notre Dame, IN, USA, [2]Department of Biological Sciences, University of Notre Dame, Notre Dame, IN, USA, [3]Lyles School of Civil Engineering, Purdue University, West Lafayette, IN, USA

Key Points:
- We link reach-scale nutrient uptake to stream geomorphic features using a continuous time random walk model
- We fit the model to conservative and reactive tracer experiments in small, unshaded experimental streams
- Using model fits, we show that rates of nutrient removal were 8 times greater in the benthic layer than in the hyporheic zone

Supporting Information:
- Supporting Information S1

Correspondence to:
K. R. Roche and A. J. Shogren,
kroche2@nd.edu;
shogrena@msu.edu

Citation:
Roche, K. R., Shogren, A. J., Aubeneau, A., Tank, J. L., & Bolster, D. (2019). Modeling benthic versus hyporheic nutrient uptake in unshaded streams with varying substrates. *Journal of Geophysical Research: Biogeosciences*, *124*, 367–383. https://doi.org/10.1029/2018JG004684

Received 3 JUL 2018
Accepted 30 DEC 2018
Accepted article online 6 JAN 2019
Published online 27 FEB 2019

Abstract Assessments of riverine ecosystem health and water quality require knowledge of how headwater streams transport and transform nutrients. Estimates of nutrient demand at the watershed scale are commonly inferred from reach-scale solute injections, which are typically reported as uptake velocities (v_f). Multiple interacting processes control v_f, making it challenging to predict how v_f responds to physical changes in the stream. In this study, we link v_f to a continuous time random walk model to quantify how v_f is controlled by in-stream (velocity, dispersion, and benthic reaction) and hyporheic processes (exchange rate, residence times, and hyporheic reaction). We fit the model to conservative (NaCl) and nitrate (NO_3^--N) pulse tracer injections in unshaded replicate streams at the Notre Dame Linked Experimental Ecosystem Facility, which differed only in substrate size and distribution. Experiments were conducted over the first 25 days of biofilm colonization to examine how the interaction between substrate type and biofilm growth influenced modeled processes and v_f. Model fits of benthic reaction rates were ~ 8× greater than hyporheic reaction rates for all experiments and did not vary with substrate type or over time. High benthic reactivity was associated with filamentous green algae coverage on the streambed, which dominated total algal biomass. Finally, v_f was most sensitive to benthic reaction rate and stream velocity, and sensitivity varied with stream conditions due to its nonlinear dependence on all modeled processes. Together, these results demonstrate how reach-scale nutrient demand reflects the relative contributions of biotic and abiotic processes in the benthic layer and the hyporheic zone.

1. Introduction

Rivers and streams regularly receive excessive nutrient loads, leading to concentrations hazardous for both ecological health and human consumption (Jaynes et al., 2001; Vitousek et al., 1997). The number of nutrient-impaired watersheds continues to grow (Galloway et al., 2008; Howarth et al., 2002), which underscores the need to understand the key physical processes governing nutrient removal from inland waters. Particularly important is an improved understanding of how headwater streams process inorganic nitrate (NO_3^--N) in intensively managed watersheds, such as those in the agricultural Midwest (USA; Alexander et al., 2007). Small headwater streams receive the majority of nonpoint-source NO_3^--N (David et al., 1997, 2010), but they naturally remove a substantial portion of these inputs before they are exported downstream (Helton et al., 2018; Mulholland et al., 2008). The high removal rate of inorganic NO_3^--N in small streams is closely linked to their underlying substrate (Peterson et al., 2001). Saturated sediments at, and just below, the sediment-water interface (SWI) provide increased surface area for microbial biofilms (Battin et al., 2016), which remove dissolved inorganic NO_3^--N from the water column via assimilation into biomass and/or dissimilatory removal via denitrification. Overall, NO_3^--N transformation is linked to biofilm biomass and metabolic activity on the stream benthos. However, knowledge of the quantity and distribution of biofilm biomass is insufficient for predicting whole-stream NO_3^--N removal, since removal depends both on biofilm demand for NO_3^--N and on its delivery to regions of the stream where demand is high (Zarnetske et al., 2015). Physical changes to the stream, such as increasing water velocity or decreasing permeability, due to biofilm clogging of stream sediments, elicit nonlinear responses in nutrient transformation rates due to covariation between nutrient transport and biofilm nutrient demand (Arnon et al., 2007; Caruso et al., 2017; Li et al., 2017; Tomasek et al., 2018). Therefore, accurate prediction of whole-stream

NO_3^--N removal requires a mechanistic understanding of how physical stream attributes controlling biofilm growth, nutrient transport, and biofilm nutrient demand covary in time.

A key driver of biofilm-mediated nutrient transformation in stream sediments is the continuous exchange of stream water and pore water, hereafter termed hyporheic exchange (Dahm et al., 1998; Valett et al., 1996). Water is driven across the SWI by natural hydraulic gradients and by turbulent velocity fluctuations (Cardenas & Wilson, 2007; Elliott & Brooks, 1997; Voermans et al., 2018). Exchange not only enhances dissolved nutrient delivery to the subsurface, but it also increases opportunities for biological uptake by greatly increasing nutrient residence times in the stream (Boano et al., 2014; Grant et al., 2018). As such, hyporheic exchange influences the rate of reach-scale nutrient transformation by setting the balance between retention and reaction timescales (Harvey et al., 2013). Natural variability of streambed elevation and sediment permeability creates spatially complex flow paths in the hyporheic zone, resulting in hyporheic residence time distributions (RTDs) that can span orders of magnitude (Berkowitz et al., 2006; Boano et al., 2007; Elliott & Brooks, 1997). The multiscale nature of hyporheic retention makes it challenging to quantify hyporheic RTDs, primarily because the full range of retention timescales typically cannot be inferred from local measurements (Fogg & Zhang, 2016). Nonetheless, the effect of multiscale retention on reach-scale transport are visible in integrated measurements, such as breakthrough curves (BTCs) measured downstream of a pulse tracer injection (Haggerty et al., 2002). Improved tracer sensitivities have revealed that BTCs commonly decay as a power law, providing a clear indication that solute residence times in the reach are similarly distributed at late times (Aubeneau et al., 2014; Haggerty et al., 2002; Stonedahl et al., 2012; Zarnetske et al., 2007). Physically based models for hyporheic exchange show that this tailing behavior is a direct consequence of solute RTDs in the hyporheic zone (Boano et al., 2014), although surface storage zones in geomorphically complex channels may retain solutes over similar timescales (Briggs et al., 2009; Jackson et al., 2013). Classical models for reach-scale transport, such as the transient storage model (Bencala & Walters, 1983), cannot capture this late-time behavior. Recent analytical models have improved the ability to predict the shape of BTCs at late times by either assuming a power law RTD in the reach (Haggerty et al., 2002; Schumer et al., 2003) or by explicitly using an RTD based on a physical description of the underlying retention processes (Boano et al., 2007).

It is critical that processes controlling hyporheic exchange and reaction are included in reach-scale models of nutrient uptake, as failure to include them can result in uncertain estimates of transport and reaction timescales compared with actual values (Bolster et al., 2017; O'Connor et al., 2010; Runkel, 2007). A popular model for describing reach-scale uptake is the nutrient spiraling model (Newbold et al., 1981; Webster & Patten, 1979). In its simplest form, this model represents nutrient uptake as an effective, first-order kinetic removal of mass as a function of downstream distance, $C(x) = C(0)e^{-x/S_w}$, where $C(x)$ is the water column concentration, x is downstream distance, and the uptake length, S_w, is the average downstream distance traveled by a solute prior to removal from the water column (Tank et al., 2017; Webster & Patten, 1979). For comparison of nutrient removal rates among streams, S_w is converted to an uptake velocity (v_f, mm/min) to account for differences in stream depths and/or velocities (Davis & Minshall, 1999; Stream Solute Workshop, 1990). As such, the spiraling model assumes that concentrations are controlled exclusively by downstream advection and first-order biological uptake (Boano et al., 2014; Webster & Patten, 1979). It therefore integrates all other processes controlling nutrient removal and transformation, such as in-stream dispersion, hyporheic exchange, and reaction rates that strongly vary across the SWI (Harvey et al., 2013; Inwood et al., 2007; Knapp et al., 2017). Integration over these additional processes masks their influence on v_f (Ensign & Doyle, 2006), particularly when they are the dominant control on nutrient removal or transformation (Hall et al., 2009).

In this study, we characterize substrate- and biofilm-driven variation in reach-scale nutrient demand (as v_f) using a continuous time random walk (CTRW) model. Use of the CTRW model is advantageous because model parameters are based on physical processes, such as stream velocity and dispersion, hyporheic exchange, and reaction rates specific to the benthic and hyporheic zones. The model is used to evaluate how these processes influence v_f in unshaded, groundwater-fed streams at the Notre Dame Linked Ecosystem Experimental Facility (ND-LEEF; Figure 1). Using sensor deployments for continuous real-time monitoring, we conducted simultaneous pulse addition experiments using NO_3^--N (as $NaNO_3$) and conservative (as NaCl) tracers. Streams were set to an initial condition with minimal biofilm growth so that they differed only in their underlying substrates, which have been previously shown to express distinct signatures of hyporheic exchange (Aubeneau et al., 2014). Five pulse additions were made in each stream over the first

25 days of biofilm colonization, allowing us to quantify how v_f was influenced by substrate type and biofilm growth. This combined experimental and modeling approach allowed us to evaluate the relative influence of in-stream and hyporheic processes on overall reach-scale NO_3^--N removal.

2. Methods

2.1. Site Description

We conducted this study in four experimental streams at ND-LEEF, located at St. Patrick's County Park, South Bend, IN, USA. Each stream is 50 m long and 0.6 m wide, with a slope of 0.0075. Streams are concrete lined so that they are isolated from groundwater gains and losses. Within each channel, the stream is lined with substrate to a depth of approximately 10 cm. As an experimental treatment, we varied substrate size and distribution among the four streams, which are pea gravel (*pg*, $D_{50} = 0.5$ cm), cobble (*cob*, $D_{50} = 5$ cm), 2-m alternating sections of *pg* and *cob* (*alt*), and one 50:50 mixture of *pg* and *cob* (*mix*; Figure 1). The ND-LEEF streams received water sourced from a groundwater-fed, constant-head reservoir with low background inorganic nutrients, where average summer concentrations are 5-μg/L ammonium, (NH_4^+-N), 4-μg/L nitrate (NO_3^--N), and 8-μg/L soluble reactive phosphorus. Experiments were performed from 18 June 2016 to 12 July 2016.

We initiated flow to the streams 2 days prior to the beginning of the experiments. Stream discharge was constant throughout the 25-day experiment to mimic baseflow conditions during a typical summer growing season. We reset the streams by removing any terrestrial organic matter (leaves, roots, etc.) and benthic algae by hand. We physically disturbed the top layer of substrate (~2–5 cm) to mobilize most remaining organic detritus, and we waited 1 day for streams to naturally flush any loose organic matter. We flattened the streambed substrate to remove any topography apart from roughness features created by sediments, which minimized transient storage in the water column at Day 0. See Aubeneau et al. (2016) and Hanrahan et al. (2018) for additional example photographs of stream substrates with and without biofilm growth.

2.2. Measurements and Solute Injection Experiments

We measured several physiochemical variables to assess the relationship between stream attributes and NO_3^--N removal. On each sampling date, we measured stream depth (d, m) as the average of 10 measurements taken along each stream reach. Before each coinjection, we collected benthic samples for estimation of algal biomass as chlorophyll *a* (chl *a*) and organic matter standing stocks (as ash-free dry mass, AFDM) every 10 m along each 50-m stream reach. We placed subsamples of substrate from a known benthic area into 160-mL specimen cups for subsequent processing in the lab. For chl *a*, we froze each subsample ($n = 5$ per stream per sampling date) and then used the methanol extraction approach in the laboratory to quantify chl *a* using a fluorometer (American Public Health Association, 2012). We then scaled each chl *a* measurement for surface area and expressed replicates in microgram chl *a* per square centimeter of streambed. We also estimated benthic organic matter by placing subsamples of each substrate type ($n = 5$ per stream per day) in ashing tins, dried for 48 hr at 60 °C and weighed after drying to obtain dry mass. We then ashed the samples at 550 °C for 1 hr and reweighed the samples. We calculated AFDM as the difference between the dry weight and ashed weight of each subsample and divided this value by the subsample surface area (38.4 cm^2) to express organic matter in microgram AFDM per square centimeter of streambed surface (Hauer & Lamberti, 2017). We visually estimated the percent cover of larger particulate organic matter types including filamentous green algae, terrestrially derived organic matter, algal biofilm, and moss along 10 transects in each stream on each sampling date.

We released chloride (as NaCl) and nitrate (as $NaNO_3$) tracers simultaneously at the upstream end of each stream reach. Injection mass for chloride was $M_c = 100$ g for all experiments; $NaNO_3$ injection mass was $M_r = 792.5$ g for each stream on Days 3 and 6 and 1,094 g on Days 10, 14, and 25. We measured chloride concentrations and average water column temperature (T, °C) every 30 s using a calibrated Hydrolab Minisonde (Hach Company, Loveland, CO), located a distance $L = 48.5$ m downstream of the injection location. We measured NO_3^--N concentration at the same location using a Sea-Bird Scientific SUNA Optical Nitrate Sensor (Bellevue, WA, USA), with an approximate sampling interval of 15 s.

2.3. Analysis of BTCs

We estimated stream discharge, Q, using standard dilution gauging, $Q = M_c / \int C_c(x,t)$, where C_c is the measured NaCl concentration and $x = L$ m was the downstream location where we measured concentrations. Uncertainty of Q was an estimated 3% (see supporting information). We calculated reactive mass recovery

Figure 1. (left) Cobble-bed (*cob*) stream with no biofilm growth (photo credit Nicole Gorman); substrates are an average of 5 cm in diameter. (upper right) Aerial view of stream with 0.5-cm pea gravels (*pg*) and no biofilm growth. (lower right) *pg* stream with biofilm coverage. Average wetted channel width is 0.6 m for all streams.

as $M_{rec} = Q \int C_r(x,t)\mathrm{d}t$, where C_r is the measured concentration of NO_3^--N. Both tracers were assumed to be transported identically, meaning any differences between normalized conservative and reactive mass recoveries were caused by biological uptake of NO_3^--N. To facilitate comparison among experiments, C_c and C_r were normalized so that conservative mass recovery is unity. We used the nutrient spiraling model (Newbold et al., 1981; Webster & Patten, 1979), adapted for pulse coinjections of conservative and reactive tracers, to quantify the characteristic distance a molecule of NO_3^--N travels downstream before it is removed from the water column, S_W (m). This model assumes an exponential decay of in-stream concentrations with downstream distance for short-term additions (i.e., steady state injections), $C(x) = C_0 e^{-x/S_W}$, where C_0 is the initial concentration of tracer released at $x = 0$. For pulse coinjections, S_W is determined from the ratio of conservative to reactive mass recovery, measured at a distance x downstream (Chapra, 2008; Tank et al., 2008). We converted S_W to an uptake velocity, v_f (mm/min), to correct for differences in discharge among experiments, $v_f = Q/(S_W w)$. Note that this equation is equivalent to $v_f = Vd/(S_w)$ under the assumption of constant stream depth and stream width, where V is the mean longitudinal velocity in the water column. We estimated the uncertainty of v_f, based on uncertainty of Q calculations, to be 4% (see supporting information).

2.4. CTRW Model for Transport and Biological Uptake

We modeled domain-specific transport and reactivity using a model based on the one-dimensional CTRW framework (Berkowitz et al., 2006; Boano et al., 2014). This model is capable of describing the wide distribution of travel times associated with solute exchange and retention in the hyporheic zone, and it has been successfully used to model conservative transport at ND-LEEF in previous studies (Aubeneau et al., 2014; 2016). The formulation used here is tailored for hyporheic exchange processes (Boano et al., 2007) and is extended to account for domain-specific (i.e., benthic and hyporheic) reaction rates (Aubeneau et al., 2015; see supporting information).

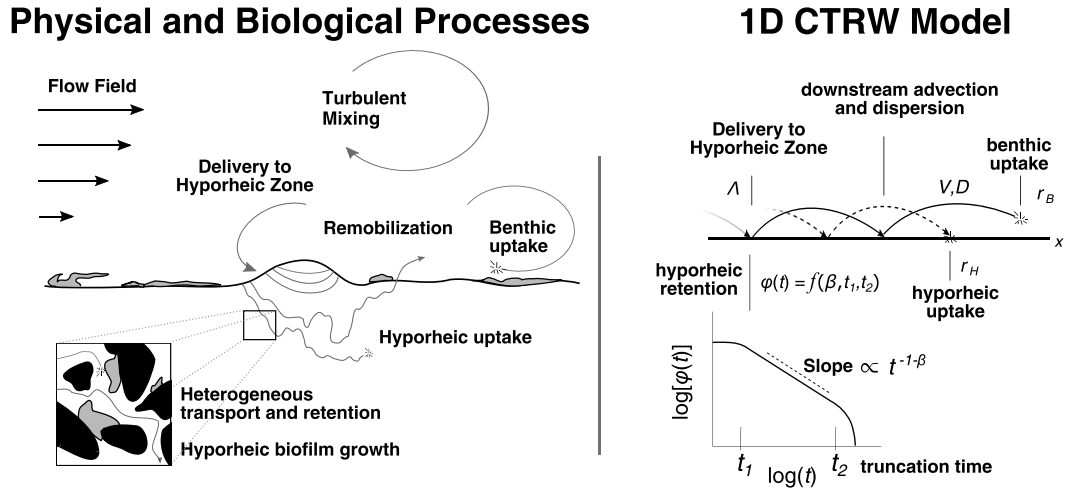

Figure 2. Conceptual diagram of modeled processes and continuous time random walk (CTRW) parameters.

In brief, the CTRW model treats the water column and hyporheic zone as a single, one-dimensional domain (Figure 2). The solute tracer is conceptualized as an ensemble of infinitesimal particles, and each particle performs a unidirectional random walk consisting of independent and identically distributed jumps and waits. In the present formulation, jumps are governed solely by the in-stream flow field and waits are controlled by retention in the hyporheic zone. This model simplification is valid when (1) processes controlling downstream transport (i.e., in-stream advection and dispersion) are independent of processes controlling subsurface residence times, which is a reasonable assumption for sand and gravel beds that do not allow for substantial penetration of turbulence; and (2) there is a large separation of velocity scales between the stream and the hyporheic zone, in which case solute retained in this zone can be considered immobile (Boano et al., 2007).

2.4.1. Transport Processes

The CTRW framework is advantageous because model parameters can be directly linked to physical processes. The two parameters controlling in-stream transport are analogous (but not equal to) to the velocity V (m/s) and dispersion D (m^2/s) in streams with impermeable beds (Boano et al., 2007). Here we conceptualize solute transfer to the hyporheic zone as a first-order exchange rate, Λ (s^{-1}), which assumes that the solute is well mixed in the water column. This assumption is reasonable in the experimental streams at ND-LEEF, because of the shallow water column (≈3 cm) and stream Reynolds numbers indicating that flows are transitional-to-turbulent ($Re \approx$ 2000–3500). Solute entering the hyporheic zone at a given time T remains immobile until it returns to the stream at time $T + t$. This retention time is a random variable sampled from an independent and identically distributed wait-time probability distribution, $\varphi(t)$, which represents the solute RTD in the hyporheic zone (Boano et al., 2007; Margolin et al., 2003). The parameter $\varphi(t)$ integrates the many mechanisms that determine hyporheic residence times into a single probability distribution (Figure 2). In streams at ND-LEEF, it is reasonable to attribute all immobilization events, and long-term retention, to storage in the hyporheic zone, since all streams are designed to minimize features that retain solutes in the water column, such as large topographic features and side cavities.

Previous experiments have shown that hyporheic residence times in ND-LEEF streams generally follow a power law distribution up to a tempering timescale, t_2, after which the distribution decays rapidly (Aubeneau et al., 2014, 2016). These dynamics can be captured by parameterizing $\varphi(\tau)$ with a truncated power law distribution (Dentz et al., 2004):

$$\varphi(t) = \{t_1(t_2/t_1)^{-\beta}\Gamma(-\beta, t_1/t_2)\}^{-1}\frac{e^{-t/t_2}}{(1+t/t_1)^{1+\beta}}, \quad (1)$$

where Γ is the upper incomplete Gamma function and β is a power law slope such that $\varphi(t) \sim t^{-\beta}$ over the interval (t_1, t_2) (Figure 2). As such, t_1 does not influence model results provided it is sufficiently small compared to other timescales in the system; it is therefore set to $t_1 = 1$ s for this study. For reasons of equifinality, we set $t_2 = 14,000$ s to match the maximum truncation time expected in ND-LEEF streams,

Table 1
CTRW Model Parameters

Parameter	Unit	Prior distribution	Description
V	m/s	0.05–0.25	Stream velocity
D	m^2/s	2E-3–0.080	Stream dispersion
Λ	s^{-1}	1E-4–0.085	Immobilization rate
β	—	0.40–1.20	RTD power law slope
t_1	s	1	RTD power law onset time
t_2	s	1.4E4	RTD power law truncation time
r_B	s^{-1}	1E-8–0.01	Benthic reaction rate
r_H	s^{-1}	1E-8–0.01	Hyporheic reaction rate

Note. The column "Prior distribution" specifies the limits of the (uniform) distribution used to initialize the $DREAM_{(ZS)}$ fitting algorithm. RTD = residence time distribution.

based on previous experiments in biofilm-covered streams (Aubeneau et al., 2016). Parameters V, D, Λ, and β thus provide a complete description of conservative solute transport at the reach scale (Figure 2).

2.4.2. Biological Uptake

We treat biological uptake of NO_3^-–N as a first-order reaction, with independent reaction rates in the benthic zone (r_B, s^{-1}) and the hyporheic zone (r_H, s^{-1}). This parameterization of reaction rates results in mathematically tractable solutions of the CTRW model, and it also allows us to compare results to traditional calculations of v_f (Stream Solute Workshop, 1990). Reactions are assumed to be uniform in each zone, which is reasonable given shallow depths for both overlying water and hyporheic zone depth (≈10 cm) that is constrained by the lining underlaying the ND-LEEF streams. First-order reactions result in exponential tempering of the wait-time distributions of conservative solutes (Aubeneau et al., 2015; Sokolov et al., 2006), leading to reaction-modified distributions $\varphi_R(t) = \varphi(t)e^{-r_i t}$, where $i \in B, H$. A list of all CTRW model parameters is provided in Table 1.

2.4.3. Model Solution and Fits

We solve the CTRW model by transforming the differential equations from the time domain to the Laplace domain, finding an algebraic solution for concentration, and then numerically transforming the solution back to the time domain (Cortis & Berkowitz, 2005; de Hoog et al., 1982). See supporting information for a full description of the reactive transport equations.

We fit model parameters using the Differential Evolution Adaptive Metropolis (DREAM) algorithm (Vrugt, 2016), which is a Bayesian estimation method based on Markov chain Monte Carlo (MCMC) simulation. The algorithm outputs a stationary posterior distribution (i.e., target distribution) of values for each model parameter. It has been previously employed in stream modeling analyses based on solute injection experiments (Knapp & Cirpka, 2017; Lemke et al., 2013). In brief, the DREAM algorithm executes a user-specified number N of parallel MCMC simulations. Parameter values for each simulation are determined from a random walk over the parameter space. A differential evolution genetic algorithm is used together with the N-chain ensemble to efficiently reach the target distribution. Here we employ the $DREAM_{(ZS)}$ algorithm, which speeds up convergence to the target distribution by incorporating information from past states of the Markov chain (Laloy & Vrugt, 2012). The $DREAM_{(ZS)}$ algorithm is publicly available as a Matlab toolbox and fully documented in Vrugt (2016).

We used a standard Bayesian formalism to condition the posterior distribution of parameters on the observed BTCs from each experiment:

$$p\left(\mathbf{a}|\tilde{\mathbf{B}}\right) \propto p\left(\mathbf{a}\right) p\left(\tilde{\mathbf{B}}|\mathbf{a}\right), \tag{2}$$

where $\mathbf{a} = \{V, D, \Lambda, \beta, r_B, r_H\}$ is the vector of free model parameters, $\tilde{\mathbf{B}}$ is the vector of observations (i.e., the concentration time series), $p\left(\mathbf{a}|\tilde{\mathbf{B}}\right)$ is the posterior distribution of parameters, $p\left(\mathbf{a}\right)$ is the prior distribution of parameters, and $p\left(\tilde{\mathbf{B}}|\mathbf{a}\right)$ is the conditional probability of observing $\tilde{\mathbf{B}}$ based on a model parameterized by $\mathbf{a}$. For conservative BTCs, parameters r_B and r_H were forced to 0.

We used $p\left(\tilde{\mathbf{B}}|\mathbf{a}\right)$ as the likelihood function, $\mathcal{L}\left(\mathbf{a}|\tilde{\mathbf{B}}\right) \equiv p\left(\tilde{\mathbf{B}}|\mathbf{a}\right)$, which describes the difference between the modeled system behavior and the observed system behavior. We treated this distance as an error term, and we assumed the error associated with each model estimate was equal to

Table 2
Biological Parameters Measured From Stream Surveys (AFDM, Chl a.), Showing Mean ±1 Standard Deviation

#	Day	Substrate	AFDM (μg/cm^2)	chl a (μg/cm^2)	Q (L/s)	v_f (mm/min)	$v_{f,model}$ (mm/min)	T (°C)
1	3	*alt*	4.8 ± 5.5	2.8 ± 1.9	0.52	2.0	2.2	15
2	3	*pg*	0.8 ± 0.3	0.7 ± 0.3	0.49	1.7	1.8	16
3	3	*mix*	6.0 ± 4.3	0.6 ± 0.4	0.62	2.3	2.5	18
4	3	*cob*	0.3 ± 0.1	2.4 ± 1.4	0.64	2.4	2.5	17
5	6	*alt*	3.3 ± 3.9	8.1 ± 5.3	0.52	2.1	2.2	18
6	6	*pg*	4.5 ± 4.8	0.8 ± 0.4	0.49	1.9	1.8	18
7	6	*mix*	14.5 ± 6.0	4.6 ± 4.8	0.62	2.6	3.0	16
8	6	*cob*	5.5 ± 2.8	4.7 ± 2.5	0.64	2.6	2.7	19
9	10	*alt*	2.7 ± 2.2	4.6 ± 2.8	0.53	2.4	2.5	19
10	10	*pg*	2.8 ± 2.6	0.8 ± 0.5	0.53	2.8	2.8	20
11	10	*mix*	2.2 ± 3.2	5.7 ± 3.7	0.66	2.6	2.8	18
12	10	*cob*	0.1 ± 0.1	5.2 ± 2.1	0.66	3.1	3.1	21
13	14	*alt*	4.6 ± 3.5	5.8 ± 1.3	0.56	2.6	2.7	23
14	14	*pg*	2.6 ± 1.6	1.1 ± 0.6	0.52	2.4	2.5	24
15	14	*mix*	0.7 ± 0.3	4.0 ± 2.0	0.65	3.0	3.2	22
16	14	*cob*	0.3 ± 0.4	3.7 ± 0.3	0.63	3.0	3.0	25
17	25	*alt*	12.7 ± 3.7	3.9 ± 1.3	0.52	2.3	2.3	29
18	25	*pg*	5.0 ± 3.5	1.3 ± 0.8	0.51	2.2	2.2	32
19	25	*mix*	2.2 ± 1.8	3.0 ± 1.2	0.58	2.5	2.6	30
20	25	*cob*	2.1 ± 2.2	3.1 ± 2.0	0.56	2.6	2.7	31

Note. Measure discharge (Q), temperature (T), and calculated and modeled v_f values for each experiment. AFDM = ash-free dry mass.

$$\mathcal{L}\left(\mathbf{a}|\tilde{\mathbf{B}}\right) = \frac{1}{n}\sum_{i=1}^{n}\left(\frac{\tilde{b}_i - b_i(\mathbf{a})}{\tilde{b}_i}\right)^2, \tag{3}$$

where $\tilde{b}_i$ is an observation from the concentration time series, $b_i(\mathbf{a})$ is a model prediction at the same time, and n is the number of observations in the time series. Equation (3) represents a nonlinear least squares algorithm (Chakraborty et al., 2009; Kelly et al., 2017), where errors are weighted by $C(t)^{-1}$. This weighting scheme, described in detail by Kelly et al. (2017), ensured that transport parameters associated with late-time solute retention and low concentrations were given a similar emphasis as in-stream transport parameters that control BTC shape at high concentrations. As a result, best fit model BTCs qualitatively captured all features of the observed reactive BTCs—that is, peak arrival time, maximum peak concentration, peak width, and tail slope. We fit the conservative and reactive BTCs from each experiment simultaneously by using the objective function

$$\min \sum_j \mathcal{L}_j\left(\mathbf{a_j}|\tilde{\mathbf{B}}_\mathbf{j}\right), j \in (\text{conservative, reactive}). \tag{4}$$

We ran eight parallel MCMC simulations that each executed the forward CTRW model 25,000 times, for a total of 200,000 model runs per experiment. We chose a uniform prior distribution for each model parameter that spanned a wide range of initial values (Table 1), with the exception of Λ. The upper limit Λ_{high} was constrained to avoid unrealistic model fits for 8 of the 20 experiments. The value of Λ_{high} was set to 0.085 s^{-1}, which is the median value of exchange rates observed in Aubeneau et al. (2016). Measured discharge in Aubeneau et al. (2016) was approximately 3× the discharge estimated for this study, which implies that the our choice of Λ_{high} was conservative (i.e., high) since exchange rates increase with water column velocity (O'Connor & Harvey, 2008). All calculations were performed in Matlab R2017b (Mathworks, Cambridge, MA).

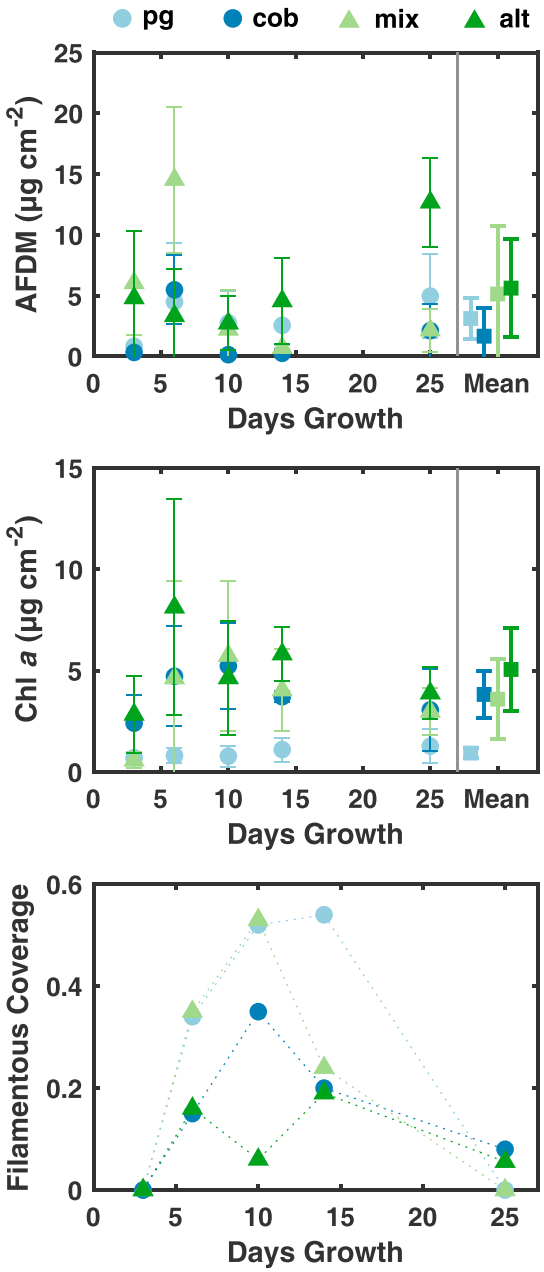

Figure 3. Biofilm measurements for all experiments. (top) Ash-free dry mass. (middle) Chlorophyll *a*. (bottom) Relative streambed coverage by filamentous green algae, calculated from stream transect surveys. See supporting information for full results from stream transect surveys. Stream abbreviations are *pg* (pea gravel), *cob* (cobble), *mix* (mixed substrate), and *alt* (alternating 2-m sections of *pg* and *cob*). AFDM = ash-free dry mass.

Early states of the Markov chain were dependent upon the chosen prior distributions during an initial burn in period. To determine when all posterior distributions had converged to their target distributions, we used the standard measure $\hat{R} \leq 1.2$, where $\hat{R}$ is a statistic that measures within-chain and between-chain variances (Gelman et al., 1992; Vrugt, 2016). We retained all N_c simulations performed after this convergence measure had been reached. The average N_c was 168,000, and $N_c \geq 112,000$ for all experiments. We report the median value of each posterior distribution as the best fit value, and we report confidence intervals as the standard deviation of each distribution.

2.4.4. Equivalence Between CTRW and Spiraling Models

Mathematically, the CTRW model solution represents the impulse response (i.e., Green's function) of a stream reach to an instantaneous tracer release. The principle of linear superposition is used with this solution to find an equivalent steady state concentration for a short-term addition experiment (see supporting information). Equivalent to the nutrient spiraling model (Newbold et al., 1981; Webster & Patten, 1979), the steady state solution for $C(x)$ is an exponentially decreasing function of downstream distance, $C_{STA}(x) = C_0 e^{-x/S_{W,model}}$, where $S_{W,model}$ (m) is the spiraling distance predicted by the CTRW model,

$$S_{W,model} = \frac{2D}{-V + \sqrt{V^2 + 4D\Theta}}, \tag{5}$$

and Θ is an expression that depends on all model parameters:

$$\Theta = r_B + \Lambda\left(1 - \frac{e^{r_H}\Gamma\left(-\beta, t_1(t_2^{-1} + r_H)\right) * \left(1 + t_2 r_H\right)^{\beta}}{\Gamma\left(-\beta, t_1/t_2\right)}\right).$$

This relation is similar to the equations presented in Runkel (2007) that link v_f to the transient storage model. The key difference between models is the underlying description of the hyporheic RTD. In Runkel (2007), the RTD is approximately exponential, while the RTD used here is based on the truncated power law distribution (equation (1)). As expected, $S_{W,model} \to \infty$ as $r_H, r_B \to 0$. We compare $S_{W,model}$ to experimental estimates by converting to model-predicted uptake velocity, $v_{f,model} = Q(S_{W,model} w)^{-1}$.

2.5. Statistical Analysis

We used a mixed effects model to evaluate how biofilm metrics differed among streams and over time (Raudenbush & Bryk, 2002). We treated colonization time as a fixed effect, and we used random intercepts for substrate treatment representing each stream. We obtained *p* values from likelihood ratio tests of the full model with the effect in question against the model in question.

We used an identical approach to assess how best fit model parameters and v_f varied with colonization time and among the four streams. Metrics that did not show significant temporal variation were treated as replicates, and differences among streams were evaluated using a one-way analysis-of-variance (ANOVA) model. If the hypothesis that metrics were equal could be rejected, we performed a Tukey's honest significant difference (HSD) test. All analyses were completed in *R* (R Core Team, 2017), and the *lmer*() function was used for mixed effects modeling (Bates et al., 2015). The script used for statistical analysis is provided with the accompanying data set (see Acknowledgments).

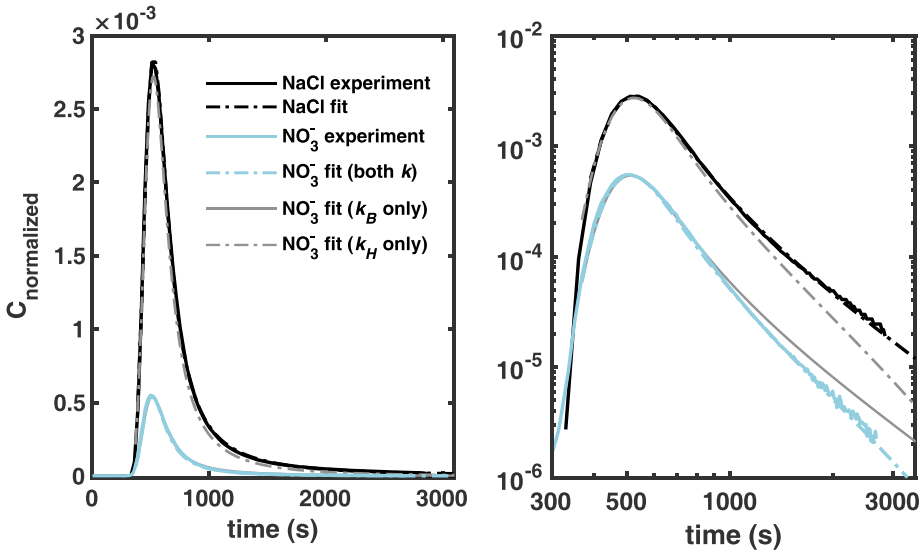

Figure 4. Example breakthrough curves and model fits for conservative (NaCl) and nutrient (NO_3^--N) tracers (black and blue lines, respectively). Concentrations are normalized so that conservative mass recovery is unity. Result is from experiment with pea gravel (*pg*) substrate and 3 days of biofilm growth. Model fits closely match observed NaCl and NO_3^--N concentrations (black and blue dashed-dotted lines, respectively). Reactive model BTCs parameterized with r_B only (i.e., $r_H = 0$, gray line) capture observed nutrient concentrations at early times ($t <\sim 800$ s) but cannot capture the more rapid concentration decrease during power law tailing (blue line). Model BTCs parameterized with r_H only (i.e., $r_B = 0$, gray dash-dotted line) do not capture the rapid concentration decrease at early times compared with the conservative BTC, but they better describe the late-time decay of observed concentrations, indicated by the identical slopes of this modeled BTC and the observed BTC (blue line).

3. Results and Discussion

3.1. Biofilm Growth

Once biofilm established, biomass metrics did not change significantly over time (mixed effects model; $\chi^2(4) = 2.17$, $p = 0.34$ for AFDM; $\chi^2(4) = 3.21$, $p = 0.52$ for chl *a*; Figure 3 and Table 2). For biofilm AFDM, small but significant differences can be seen between *cob* and *alt*, as well as between *cob* and *mix* streams, but no other differences were significant (one-way ANOVA, $p < 0.001$, Tukey HSD $p < 0.05$ for both). For biofilm chl *a*, we only found differences between *pg* and all other streams (one-way ANOVA, $p < 0.001$, Tukey HSD $p < 0.01$ for both). These results are similar to those reported by Hanrahan et al. (2018), which showed that large differences in biomass metrics did not emerge among stream substrate treatments until after 4–6 weeks of biofilm colonization. In contrast to biofilm metrics, mixed model results showed that relative coverage of filamentous green algae varied significantly over time ($\chi^2(2) = 16.32$, $p < 0.001$), with as much as half the stream bed covered in *pg* and *mix* streams between Days 10 and 14. Filamentous algae coverage then declined rapidly to <10% by Day 25 (Figure 3), as a result of a heat wave that increased water column temperature from 23.5 °C on day 15 to 30.5 °C on Day 25. Filamentous green algae primarily grew into the water column as long strands tethered both to the substrate and to channel sidewalls. As such, biomass metrics of AFDM and chl *a* did not parallel the trends in filamentous green algae growth because they measured biofilm biomass at and below the SWI.

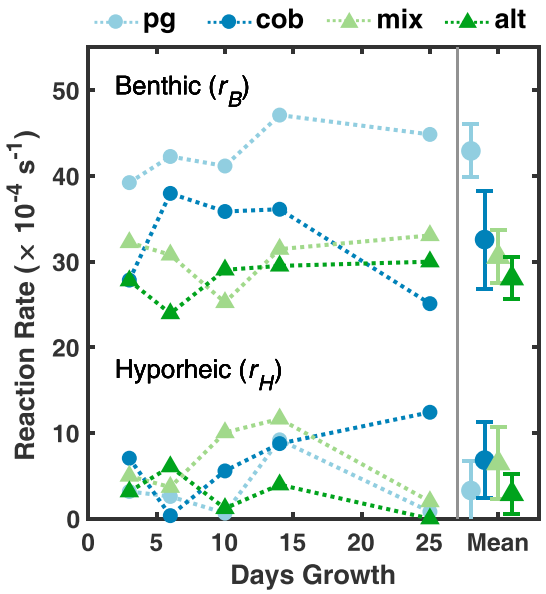

Figure 5. Best fit model values for benthic (r_B) and hyporheic (r_H) reaction rates. Stream abbreviations are *pg* (pea gravel), *cob* (cobble), *mix* (mixed substrate), and *alt* (alternating 2-m sections of *pg* and *cob*).

3.2. CTRW Model Fits

We present example BTCs and corresponding CTRW model fits in Figure 4. Both conservative (NaCl) and nutrient (NO_3^--N) tracer concentrations decayed to near-background levels 2,600–3,900 s after each pulse release, with the onset of power law tailing occurring after approximately

Table 3
Continuous Time Random Walk Model Fits For All Experiments

#	Day	Sub	V ($\times 10^{-2}$ m/s)	D ($\times 10^{-2}$ m^2/s)	Λ ($\times 10^{-2}$ s^{-1})	β (—)	r_B ($\times 10^{-4}$ s^{-1})	r_H ($\times 10^{-4}$ s^{-1})	r_B/r_H (—)
1	3	*alt*	07.39 ± 0.00	1.84 ± 0.01	8.50*	0.87 ± 0.00	27.78 ± 0.04	03.15 ± 0.05	8.8E0
2	3	*pg*	11.34 ± 0.03	3.78 ± 0.03	4.67 ± 0.06	0.75 ± 0.00	39.22 ± 0.09	03.17 ± 0.06	1.2E1
3	3	*mix*	08.98 ± 0.01	2.63 ± 0.01	2.32 ± 0.03	0.57 ± 0.00	32.24 ± 0.05	04.98 ± 0.06	6.5E0
4	3	*cob*	08.28 ± 0.03	2.66 ± 0.02	4.83 ± 0.09	0.76 ± 0.00	27.84 ± 0.07	07.06 ± 0.06	3.9E0
5	6	*alt*	06.70 ± 0.00	1.23 ± 0.01	8.50*	0.88 ± 0.00	23.94 ± 0.05	06.07 ± 0.05	3.9E0
6	6	*pg*	11.21 ± 0.00	0.85 ± 0.01	8.50*	0.87 ± 0.00	42.27 ± 0.06	02.59 ± 0.06	1.6E1
7	6	*mix*	07.27 ± 0.01	0.58 ± 0.01	3.88 ± 0.04	0.73 ± 0.00	30.79 ± 0.06	03.68 ± 0.05	8.4E0
8	6	*cob*	09.21 ± 0.00	2.06 ± 0.01	8.50*	0.85 ± 0.00	37.96 ± 0.05	00.35 ± 0.06	1.1E2
9	10	*alt*	06.51 ± 0.03	1.55 ± 0.01	5.60 ± 0.13	0.80 ± 0.00	29.04 ± 0.12	01.20 ± 0.05	2.4E1
10	10	*pg*	08.05 ± 0.02	0.27 ± 0.01	7.31 ± 0.08	0.89 ± 0.00	41.89 ± 0.09	00.74 ± 0.07	5.7E1
11	10	*mix*	07.08 ± 0.01	1.40 ± 0.01	1.74 ± 0.02	0.57 ± 0.00	25.24 ± 0.04	10.05 ± 0.10	2.5E0
12	10	*cob*	08.53 ± 0.00	2.39 ± 0.01	8.50*	0.86 ± 0.00	35.85 ± 0.06	05.57 ± 0.07	6.4E0
13	14	*alt*	06.86 ± 0.00	1.38 ± 0.01	8.50*	0.92 ± 0.00	29.50 ± 0.05	03.96 ± 0.07	7.4E0
14	14	*pg*	11.52 ± 0.02	2.46 ± 0.02	4.70 ± 0.05	0.72 ± 0.00	47.10 ± 0.09	09.21 ± 0.10	5.1E0
15	14	*mix*	07.42 ± 0.01	1.74 ± 0.01	1.85 ± 0.03	0.62 ± 0.00	31.46 ± 0.04	11.65 ± 0.13	2.7E0
16	14	*cob*	09.07 ± 0.00	3.61 ± 0.01	8.50*	0.84 ± 0.00	36.11 ± 0.07	08.76 ± 0.09	4.1E0
17	25	*alt*	06.85 ± 0.00	1.41 ± 0.01	8.50*	0.92 ± 0.00	29.99 ± 0.03	00.00 ± 0.00	5.2E4
18	25	*pg*	10.54 ± 0.02	2.00 ± 0.01	4.07 ± 0.05	0.78 ± 0.00	44.84 ± 0.08	00.82 ± 0.08	5.5E1
19	25	*mix*	07.68 ± 0.01	1.84 ± 0.01	2.17 ± 0.03	0.68 ± 0.00	33.05 ± 0.05	02.00 ± 0.08	1.7E1
20	25	*cob*	07.01 ± 0.03	1.26 ± 0.01	8.39 ± 0.15	0.89 ± 0.00	25.09 ± 0.07	12.42 ± 0.12	2.0E0

Note. Variables are defined in Table 1. Reported values are the median of posterior parameter distributions, with uncertainty values showing one standard deviation. Best fit values that are constrained by the prior distribution are marked with an asterisk (*).

1,000–1,200 s. Model fits to nutrient BTCs required independent estimates of benthic and hyporheic reaction rates (r_B and r_H, respectively), indicating that both the benthic and hyporheic zones made measurable contributions to reach-scale NO_3^--N removal in ND-LEEF streams. Further, the omission of either parameter resulted in systematic differences between the modeled and observed BTCs (Figure 4). We also found that r_B controlled the shape of modeled BTCs at early times ($t <\sim 800$ s), while a nonzero value for r_H was needed to capture the steeper power law slope observed in the nutrient BTC at late times ($t >\sim 1,000$ s), compared with the slope of the conservative BTC (Figure 4).

Best fit model parameters showed no significant correlations over time or with biofilm metrics (mixed effects model, $p > 0.05$ for all; Table 3). In general, there were no significant differences among streams (one-way ANOVA, $p > 0.05$), with the exception of higher V in the *pg* stream (Tukey HSD, $p < 0.05$), lower Λ and β in the *mix* stream ($p < 0.01$), and higher r_B in the *pg* stream (Tukey HSD, $p < 0.001$). These results differed slightly from those reported in Aubeneau et al. (2016), who found qualitative differences in BTCs among streams over the first 3 weeks of the biofilm colonization sequence. We suggest that the contrasting results were most likely due to differences in initial conditions; experiments in Aubeneau et al. (2016) began immediately after new rock substrate was installed in the ND-LEEF streams. Although the same substrate types were used in the present study, they had in-filled with some organic detritus following a full growing season from the previous year, which likely tempered differences among substrate treatments. Additionally, temporal changes to BTCs reported in Aubeneau et al. (2016) were most pronounced in the truncation time (t_2) and the power law slope (β). The lower signal-to-noise ratio of NaCl tracer used here, compared with Rhodamine-WT tracer used in Aubeneau et al. (2016), limited the late-time resolution of BTCs in this study, meaning small changes to β were not detectable. Nonetheless, CTRW model fits accurately described conservative concentrations across all observation times (e.g., Figure 4). Estimates of r_B/r_H were greater than 1 for all experiments, with a median value of $r_B/r_H \sim 8$ and a range of 2.0-52,000 (Table 3 and Figure 5).

Posterior distributions of model parameters were narrow and symmetric, indicating that the fitting algorithm had achieved a global minimum of the objective function (see Table 3 and supporting information).

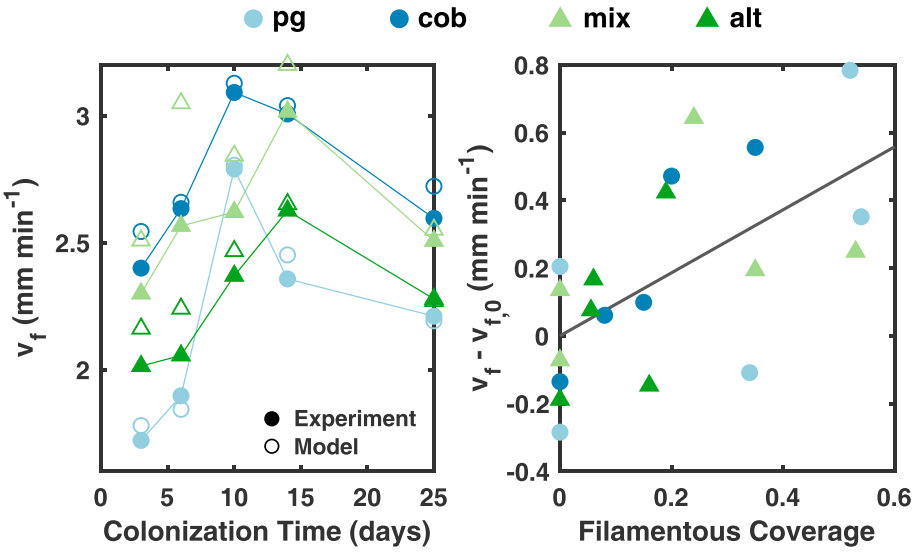

Figure 6. (left) Measured and modeled uptake velocities v_f for all experiments. Hollow symbols represent the predicted estimate $v_{f,model}$ (equation (5)). (right) v_f correlated with streambed filamentous green algae coverage (linear mixed model, $\chi^2(2) = 16.32, p < 0.001$). The y-axis shows v_f values corrected by the mixed model's predicted intercept, which is equal to the mean v_f observed for all experiments with zero filamentous green algae coverage. $v_{f,0} = 2.01(pg); 2.54(cob); 2.37(mix); 2.20(alt)$ mm/min. The predicted model slope of 0.93 mm·min^{-1}·(frac. coverage)$^{-1}$ is shown in black. Stream abbreviations are *pg* (pea gravel), *cob* (cobble), *mix* (mixed substrate), and *alt* (alternating 2-m sections of *pg* and *cob*).

Estimates for Λ were forced to the upper constraint $\Lambda_{\text{high}} = 0.085$ s^{-1} in eight experiments (Table 3), and increases to Λ_{high} increased the model fits to values that were considered unphysical based on findings from previous studies (Aubeneau et al., 2014, 2016). Although constrained parameters showed a weak, positive correlation with r_B, model fits to a distribution with larger Λ_{high} did not substantially alter the relative magnitudes of r_B and r_H. This result supports our conclusion that benthic reaction rates were higher in all experiments (see supporting information).

3.3. Reach-Scale Nutrient Uptake: Measured Values

The integrated effects of transport and reaction were reflected in measures of uptake velocity, v_f (Figure 6). Calculated v_f values ranged from 1.7–3.1 mm/min, with an estimated uncertainty of ±0.1 mm/min based on uncertainty of Q calculations (see supporting information). This v_f range was higher than the range of 1.2–2.0 mm/min reported for NO_3^--N in Hanrahan et al. (2018), who conducted short-term nutrient additions over 16 weeks of biofilm colonization. The difference is most likely due to benthic substrate in Hanrahan et al. (2018) being initially free of organic matter or biofilms, while as mentioned above, the benthic substrate in this study had some infilling from legacy detritus from the previous growing season, which likely contributed to the microbial demand for NO_3^--N.

We found that v_f differed significantly across sampling dates ($\chi^2(2) = 22.71$, $p < 0.001$), with highest nutrient demand peaking between Days 10 and 15 and falling sharply by Day 25. Additionally, v_f correlated significantly with relative coverage of filamentous green algae ($\chi^2(1) = 6.46, p = 0.011$, Figure 6), which dominated algal biomass (see supporting information), suggesting that filamentous algae dominated NO_3^--N demand in ND-LEEF streams. These results are consistent with previous studies demonstrating the role of filamentous algae for NO_3^--N uptake in open-canopy streams (Kemp & Dodds, 2002). We also suggest that the lack of relationship between v_f and biofilm AFDM or chl *a* was likely because biofilms represent a relatively small proportion of biomass relative to filamentous green algae in these systems.

3.4. Reach-Scale Nutrient Uptake: Model Results

Modeled estimates of uptake velocity, $v_{f,model}$, were within 5% of measured values, demonstrating that the CTRW model reasonably described the integrated effects of transport and reaction in ND-LEEF streams

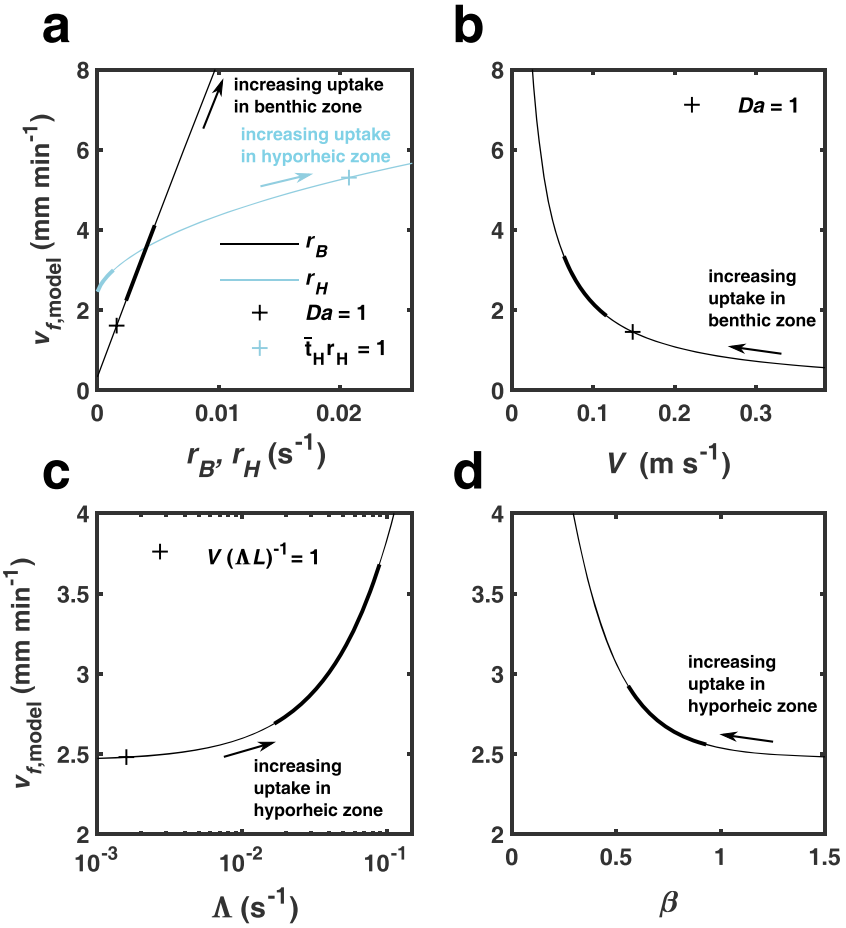

Figure 7. Parameter $v_{f,model}$ exhibits nonlinear sensitivity to all CTRW model parameters over the range of best fit values observed from experiments, with the exception of r_B. Analysis is based on mean values of all model fits from the mixed sediment (*mix*) stream. Bold lines represent the range of best fit values for all experiments. Note the difference in the *y*-axis between top and bottom plots.

(Figure 6). The relative influence of each model parameter is illustrated in Figure 7. This figure shows calculations of $v_{f,model}$ using the average parameter values from releases in *mix* streams as a representative sample. Plots show the response of $v_{f,model}$ to changes in one free parameter, with all other free parameters held constant. Over the range of values determined from model fits (Figure 7, thick lines), $v_{f,model}$ exhibits the greatest range of values in response to changes in-stream advection (V) and benthic reactivity (r_B). The range of $v_{f,model}$ values resulting from changes in r_B was 3.4× greater than the range resulting from changes in r_H. Although this outcome is reasonable given that benthic reactivity is much higher than hyporheic reactivity, codependence of $v_{f,model}$ on all parameters (equation (5)) suggests that a balance of transport- and reaction-related processes determines the relative sensitivity of v_f to any specific process. A common metric for evaluating this balance is the nondimensional Damköhler number, $Da = \tau_T/\tau_R$, which provides a direct comparison between transport and reaction timescales (τ_T and τ_R, respectively). In a stream with relatively fast reaction rates, $Da \gg 1$, nutrient removal is limited by the characteristic time spent in the water column (i.e., transport-limited conditions), and $v_{f,model}$ sensitivity to changes in reactivity is low. In contrast, $Da \ll 1$ when uptake is limited by reaction rates, and changes in reactivity are expected to produce a relatively large response in $v_{f,model}$. A transition from transport-limited to reaction-limited conditions occurs near $Da \sim 1$, which can result in a nonlinear sensitivity of v_f to changes in a specific process. Here τ_T is set to the characteristic travel time through the reach, $\tau_T = L V^{-1}$, and τ_R is set to the e-folding time for benthic reaction, $\tau_R = r_B^{-1}$. In Figures 7a and 7b, *Da* values are slightly greater than 1 over the range of best fit parameters (thick black lines). As a result, $v_{f,model}$ is sensitive to both transport- and reaction-related parameters in the water column, and $v_{f,model}$ responds nonlinearly over the range of velocities inferred from model fits.

We do not calculate a Damköhler number associated with hyporheic processes, since the principal model assumption that solute residing in the hyporheic zone is immobile precludes the existence of a transport timescale. Nonetheless, $v_{f,model}$ sensitivity to hyporheic exchange-related parameters can be interpreted by evaluating how these parameters increase the cumulative opportunity for hyporheic uptake in the reach. Uptake velocity is sensitive to r_H until the mean hyporheic zone residence time, $\overline{t_H}$, exceeds the characteristic reaction time in the zone, that is, $\overline{t_H} r_H > 1$. Beyond this value, reactions occur within the hyporheic zone over shorter timescales than the mean residence time, and $v_{f,model}$ sensitivity to r_H decreases with increasing r_H. In Figures 7a, 7c, and 7d, $v_{f,model}$ increases nonlinearly from a value of 2.56 mm/min, which is equal to the uptake velocity in an equivalent stream with no hyporheic exchange and/or hyporheic reactions. This uptake velocity is reached in Figure 7c when the mean residence time in the water column ($\overline{t_B} = \Lambda^{-1}$) is approximately equal to τ_T, that is, $V(\Lambda L)^{-1} = 1$, signifying that immobilization events are too seldom to result in substantial uptake in the hyporheic zone. Similarly, increasing β reduces hyporheic residence times until they are too short for reactions to progress before solute is remobilized. (In Figure 7d, $v_{f,model}$ falls within 5% of 2.56 mm/min when the mean hyporheic residence time is within 1% of r_B^{-1}.)

Linkage of v_f to the CTRW model may potentially improve analysis of cross-stream studies since CTRW model parameters are often directly related to measurable stream processes (Aubeneau et al., 2015; Boano et al., 2007; Drummond et al., 2018). Model-based estimates of these processes may aid interpretation of the factors that control them via a direct comparison with stream measurements. For example, using ^{15}N tracer additions, biomass metrics, and compartment-specific estimates of N storage, Tank et al. (2018) showed that canopy cover strongly drives reach-scale inorganic N uptake by influencing the abundance and activity of primary producers. Our results show that pulse addition tracer experiments, together with CTRW model fits, can provide an additional estimate of primary producer activity (as r_b) when they control benthic NO_3^--N demand. Not only can model results be compared with local estimates of benthic uptake in open-canopy and shaded reaches (Tank et al., 2018), but they can also be used to effectively quantify how the relative influence of r_b on v_f varies with differences in overall cover, compared to the other modeled processes.

3.5. Limitations

Very narrow posterior distributions indicate that the $DREAM_{(ZS)}$ algorithm had reached a global optimum set of parameters for each experiment. Nonetheless, best fit model parameters associated with solute transport (V, D, Λ, β) varied widely among experiments. For instance, although CTRW model fits described conservative BTCs well in streams with pea gravel, fits of V, D, and Λ varied by 25–85% for consecutive experiments between Days 3 and 10 (see Table 3 and supporting information). It is unlikely that such high variability is due to physical variation in the stream since stream discharge was well controlled. Fits to the Day 3 *pg* experiment yielded best fit values closer to their true values since BTCs from this experiment exhibited a pronounced interval of power law tailing, compared to other experiments in the same stream (Table 3 and Figure 4).

High variability of transport model parameters is hypothesized to be a consequence of limited observation of long-term retention processes. Model fits of V, D, Λ, and β likely had not converged to values independent of BTC length since BTCs lacked a sufficiently long interval of power law tailing to properly constrain β. This point is further evidenced by strong correlations between transport model parameters (see supporting information), meaning fits to these parameters remained correlated if BTCs were too short to capture a pronounced interval of power law tailing. Data limitation is therefore a source of model equifinality for the present experiments, creating unphysical variability of best fit transport model parameters and masking any correlations that may exist between these parameters and biofilm growth metrics. In contrast, fits to reactive model parameters showed lower covariation with transport parameters and varied less than transport parameters across time (see supporting information), which supports our conclusion that $r_B > r_H$ in ND-LEEF streams (Figure 5).

The nonlinear dependence of v_f on all model parameters suggests that changes to any specific process can alter its influence relative to others (equation (5)), particularly for changes resulting in a transition from reaction-dominant to transport-dominant conditions (or vice versa, see Figure 7). Our results demonstrate how fits to a CTRW model with reactions can be used to quantify the range of stream conditions where this transition will occur. Nonetheless, we expect further covariation between transport and reaction processes that are not described by the current CTRW model formulation. Increases in discharge, for example, simultaneously alter the water column velocity profile, enhance exchange rates, and modify the distribu-

tion of hyporheic residence times (Grant et al., 2012; Manes et al., 2009; Nissan & Berkowitz, 2018). These changes can subsequently alter subsurface redox conditions and assimilatory versus respiratory demand for NO_3^--N (Briggs et al., 2015; Kaufman et al., 2017; Tomasek et al., 2018). Experimental results from a single flow rate or substrate treatment therefore cannot be generalized without an improved understanding of how specific processes are coupled. Future studies are needed in order to identify the mechanistic controls on process coupling and whether these additional controls satisfy or violate the assumptions underlying the mobile-immobile CTRW model (e.g., Aubeneau et al., 2015).

4. Conclusions and Implications

The approach and results presented here demonstrate the relative importance of in-stream and hyporheic processes in determining overall NO_3^--N demand by explicitly quantifying their influence on v_f (equation (5)). Results from controlled experiments in replicated experimental streams at ND-LEEF show that v_f was over 3× more sensitive to changes in benthic reaction rates than to changes in hyporheic zone reaction rates (based on modeled v_f over the range of best fit reaction rates). Coverage of filamentous algae was significantly correlated with experimentally measured v_f, which suggests that high NO_3^--N removal from the water column was attributable to algal demand for inorganic N. Together, these results support previous findings that NO_3^--N uptake in low-nutrient streams is closely linked to primary production (Hall & Tank, 2003; Kemp & Dodds, 2002; Mulholland et al., 2008) and that processes associated with hyporheic transformation, such as assimilation by hyporheic biofilms and microbially mediated denitrification, played a minor role in removing NO_3^--N from the water column over hourly timescales. Future studies can build on these results through the use of ^{15}N tracer additions that would allow short-term inorganic N removal to be partitioned into its contributing processes, such as assimilatory uptake into biomass, remineralization, denitrification, and longer-term hyporheic storage (Findlay et al., 2011; Hall et al., 2009; Mulholland et al., 2000; Tank et al., 2018).

A strength of the combined experimental and modeling approach used here is that it provides domain-specific insights into the general processes influencing solute uptake, while using similar methods to those established previously for experimental field studies (Tank et al., 2017). Model results can be used to identify where costly or time-intensive experimental efforts should be directed, such as local assays of benthic NO_3^--N demand (Reisinger et al., 2016) versus detailed measures of NO_3^--N transformation in the hyporheic zone (Harvey et al., 2013; Zarnetske et al., 2011). Insights gleaned from local measurements can also be linked directly to model parameters (Boano et al., 2007; Drummond et al., 2014; Roche et al., 2017), making the CTRW framework a valuable tool for assessing how local processes will impact nutrient removal and transformation at the reach scale.

Acknowledgments
Brett Peters and Nicole Gorman are gratefully acknowledged for assisting with field experiments and biofilm analysis in the lab. We also thank Marc Müller for assistance with the statistical analysis. This work was supported in part by the Biotechnology Risk Assessment Grants (BRAG) program from the U.S. Department of Agriculture, under award number (USDA 2016-33522-25629). K. R. R. and D. B. also gratefully acknowledge funding support from NSF via grants EAR-1351625 and CBET-1705770. We acknowledge two anonymous reviewers for helping us substantially improve the quality of this manuscript. See supporting information for a detailed description of the CTRW model derivation, plots of all experimental BTCs, and uncertainty analysis. Data and R scripts used for statistical analysis are accessible at https://doi.org/10.7274/R0XW4GW9.

References

American Public Health Association (2012). Standard methods for the examination of water and wastewater.

Alexander, R. B., Boyer, E. W., Smith, R. A., Schwarz, G. E., & Moore, R. B. (2007). The role of headwater streams in downstream water quality 1. *JAWRA Journal of the American Water Resources Association*, *43*, 41–59. https://doi.org/10.1111/j.1752-1688.2007.00005.x

Arnon, S., Peterson, C. G., Gray, K. A., & Packman, A. I. (2007). Influence of flow conditions and system geometry on nitrate use by benthic biofilms: Implications for nutrient mitigation. *Environmental science & technology*, *41*, 8142–8148.

Aubeneau, A. F., Drummond, J. D., Schumer, R., Bolster, D., Tank, J. L., & Packman, A. I. (2015). Effects of benthic and hyporheic reactive transport on breakthrough curves. *Freshwater Science*, *34*, 301–315.

Aubeneau, A. F., Hanrahan, B., Bolster, D., & Tank, J. L. (2014). Substrate size and heterogeneity control anomalous transport in small streams. *Geophysical Research Letters*, *41*, 8335–8341. https://doi.org/10.1002/2014GL061838

Aubeneau, A. F., Hanrahan, B., Bolster, D., & Tank, J. (2016). Biofilm growth in gravel bed streams controls solute residence time distributions. *Journal of Geophysical Research: Biogeosciences*, *121*, 1840–1850. https://doi.org/10.1002/2016JG003333

Bates, D., Mächler, M., Bolker, B., & Walker, S. (2015). Fitting linear mixed-effects models using lme4. *Journal of Statistical Software*, *67*, 1–48.

Battin, T. J., Besemer, K., Bengtsson, M. M., Romani, A. M., & Packmann, A. I. (2016). The ecology and biogeochemistry of stream biofilms. *Nature Reviews Microbiology*, *14*, 251.

Bencala, K. E., & Walters, R. A. (1983). Simulation of solute transport in a mountain pool-and-riffle stream: A transient storage model. *Water Resources Research*, *19*, 718–724. https://doi.org/10.1029/WR019i003p00718

Berkowitz, B., Cortis, A., Dentz, M., & Scher, H. (2006). Modeling non-Fickian transport in geological formations as a continuous time random walk. *Reviews of Geophysics*, *44*, RG2003. https://doi.org/10.1029/2005RG000178

Boano, F., Harvey, J. W., Marion, A., Packman, A. I., Revelli, R., Ridolfi, L., & Wörman, A. (2014). Hyporheic flow and transport processes: Mechanisms, models, and biogeochemical implications. *Reviews of Geophysics*, *52*, 603–679. https://doi.org/10.1002/2012RG000417

Boano, F., Packman, A., Cortis, A., Revelli, R., & Ridolfi, L. (2007). A continuous time random walk approach to the stream transport of solutes. *Water Resources Research*, *43*, W10425. http://www.agu.org/pubs/crossref/2007/2007WR006062.shtml

Bolster, D., Benson, D. A., & Singha, K. (2017). Upscaling chemical reactions in multicontinuum systems: When might time fractional equations work? *Chaos, Solitons & Fractals*, *102*, 414–425. http://www.sciencedirect.com/science/article/pii/S0960077917301637, Future Directions in Fractional Calculus Research and Applications.

Briggs, M. A., Day-Lewis, F. D., Zarnetske, J. P., & Harvey, J. W. (2015). A physical explanation for the development of redox microzones in hyporheic flow. *Geophysical Research Letters*, *42*, 4402–4410. https://doi.org/10.1002/2015GL064200

Briggs, M. A., Gooseff, M. N., Arp, C. D., & Baker, M. A. (2009). A method for estimating surface transient storage parameters for streams with concurrent hyporheic storage. *Water Resources Research*, *45*, W00D27. https://doi.org/10.1029/2008WR006959

Cardenas, M. B., & Wilson, J. L. (2007). Dunes, turbulent eddies, and interfacial exchange with permeable sediments. *Water Resources Research*, *43*, W08412. https://doi.org/10.1029/2006WR005787

Caruso, A., Boano, F., Ridolfi, L., Chopp, D. L., & Packman, A. (2017). Biofilm-induced bioclogging produces sharp interfaces in hyporheic flow, redox conditions, and microbial community structure. *Geophysical Research Letters*, *44*, 4917–4925. https://doi.org/10.1002/2017GL073651

Chakraborty, P., Meerschaert, M. M., & Lim, C. Y. (2009). Parameter estimation for fractional transport: A particle-tracking approach. *Water Resources Research*, *45*, W10415. https://doi.org/10.1029/2008WR007577

Chapra, S. C. (2008). *Surface water-quality modeling*. Long Grove, IL: Waveland Press Inc.

Cortis, A., & Berkowitz, B. (2005). Computing "anomalous" contaminant transport in porous media: The CTRW MATLAB toolbox. *Groundwater*, *43*, 947–950.

Dahm, C. N., Grimm, N. B., Marmonier, P., Valett, H. M., & Vervier, P. (1998). Nutrient dynamics at the interface between surface waters and groundwaters. *Freshwater Biology*, *40*, 427–451. https://doi.org/10.1046/j.1365-2427.1998.00367.x

David, M. B., Drinkwater, L. E., & McIsaac, G. F. (2010). Sources of nitrate yields in the Mississippi River basin. *Journal of Environmental Quality*, *39*, 1657–1667.

David, M. B., Gentry, L. E., Kovacic, D. A., & Smith, K. M. (1997). Nitrogen balance in and export from an agricultural watershed. *Journal of Environmental Quality*, *26*, 1038–1048.

Davis, J. C., & Minshall, G. W. (1999). Nitrogen and phosphorus uptake in two Idaho (USA) headwater wilderness streams. *Oecologia*, *2*, 247–255.

de Hoog, F., Knight, J., & Stokes, A. (1982). An improved method for numerical inversion of Laplace transforms. *SIAM Journal on Scientific and Statistical Computing*, *3*, 357–366.

Dentz, M., Cortis, A., Scher, H., & Berkowitz, B. (2004). Time behavior of solute transport in heterogeneous media: Transition from anomalous to normal transport. *Advances in Water Resources*, *27*, 155–173. http://www.sciencedirect.com/science/article/pii/S0309170803001726

Drummond, J., Aubeneau, A., & Packman, A. (2014). Stochastic modeling of fine particulate organic carbon dynamics in rivers. *Water Resources Research*, *50*, 4341–4356. https://doi.org/10.1002/2013WR014665

Drummond, J. D., Larsen, L. G., González-Pinzón, R., Packman, A. I., & Harvey, J. W. (2018). Less fine particle retention in a restored versus unrestored urban stream: Balance between hyporheic exchange, resuspension, and immobilization. *Journal of Geophysical Research: Biogeosciences*, *123*, 1425–1439. https://doi.org/10.1029/2017JG004212

Elliott, A. H., & Brooks, N. H. (1997). Transfer of nonsorbing solutes to a streambed with bed forms: Theory. *Water Resources Research*, *33*, 123–136.

Ensign, S. H., & Doyle, M. W. (2006). Nutrient spiraling in streams and river networks. *Journal of Geophysical Research*, *111*, G04009. https://doi.org/10.1029/2005JG000114

Findlay, S. E. G., Mulholland, P. J., Hamilton, S. K., Tank, J. L., Bernot, M. J., Burgin, A. J., et al. (2011). Cross-stream comparison of substrate-specific denitrification potential. *Biogeochemistry*, *104*, 381–392. https://doi.org/10.1007/s10533-010-9512-8

Fogg, G. E., & Zhang, Y. (2016). Debates–stochastic subsurface hydrology from theory to practice: A geologic perspective. *Water Resources Research*, *52*, 9235–9245. https://doi.org/10.1002/2016WR019699

Galloway, J. N., Townsend, A. R., Erisman, J. W., Bekunda, M., Cai, Z., Freney, J. R., et al. (2008). Transformation of the nitrogen cycle: Recent trends, questions, and potential solutions. *Science*, *320*, 889–892. http://science.sciencemag.org/content/320/5878/889

Gelman, A., & Rubin, D. B. (1992). Inference from iterative simulation using multiple sequences. *Statistical Science*, *7*, 457–472.

Grant, S. B., Azizian, M., Cook, P., Boano, F., & Rippy, M. A. (2018). Factoring stream turbulence into global assessments of nitrogen pollution. *Science*, *359*, 1266–1269. http://science.sciencemag.org/content/359/6381/1266

Grant, S. B., Stewardson, M. J., & Marusic, I. (2012). Effective diffusivity and mass flux across the sediment-water interface in streams. *Water Resources Research*, *48*, W05548. https://doi.org/10.1029/2011WR011148

Haggerty, R., Wondzell, S. M., & Johnson, M. A. (2002). Power-law residence time distribution in the hyporheic zone of a 2nd-order mountain stream. *Geophysical Research Letters*, *29*(13), 1640. https://doi.org/10.1029/2002GL014743

Hall, R. O. Jr., Baker, M. A., Arp, C. D., & Koch, B. J. (2009). Hydrologic control of nitrogen removal, storage, and export in a mountain stream. *Limnology and Oceanography*, *54*, 2128–2142. https://doi.org/10.4319/lo.2003.48.3.1120

Hall, R. O. Jr., & Tank, J. L. (2003). Ecosystem metabolism controls nitrogen uptake in streams in Grand Teton National Park, Wyoming. *Limnology and Oceanography*, *48*, 1120–1128.

Hanrahan, B., Tank, J., Aubeneau, A. F., & Bolster, C. (2018). Substrate-specific biofilms control nutrient uptake in experimental streams. *Freshwater Science*, *37*, 456–471. https://doi.org/10.1086/699004

Harvey, J. W., Böhlke, J. K., Voytek, M. A., Scott, D., & Tobias, C. R. (2013). Hyporheic zone denitrification: Controls on effective reaction depth and contribution to whole-stream mass balance. *Water Resources Research*, *49*, 6298–6316. https://doi.org/10.1002/wrcr.20492

Hauer, F. R., & Lamberti, G. (2017). *Methods in stream ecology: Volume 1: Ecosystem structure*. Cambridge, MA: Academic Press.

Helton, A. M., Hall, R. O., & Bertuzzo, E. (2018). How network structure can affect nitrogen removal by streams. *Freshwater Biology*, *63*, 128–140. https://doi.org/10.1111/fwb.12990

Howarth, R. W., Boyer, E. W., Pabich, W. J., & Galloway, J. N. (2002). Nitrogen use in the United States from 1961–2000 and potential future trends. *AMBIO: A Journal of the Human Environment*, *31*, 88–96.

Inwood, S. E., Tank, J. L., & Bernot, M. J. (2007). Factors controlling sediment denitrification in midwestern streams of varying land use. *Microbial Ecology*, *53*, 247–258. https://doi.org/10.1007/s00248-006-9104-2

Jackson, T. R., Haggerty, R., & Apte, S. V. (2013). A fluid-mechanics based classification scheme for surface transient storage in riverine environments: Quantitatively separating surface from hyporheic transient storage.

Jaynes, D., Colvin, T., Karlen, D., Cambardella, C., & Meek, D. (2001). Nitrate loss in subsurface drainage as affected by nitrogen fertilizer rate. *Journal of Environmental Quality*, *30*, 1305–1314.

Kaufman, M. H., Cardenas, M. B., Buttles, J., Kessler, A. J., & Cook, P. L. M. (2017). Hyporheic hot moments: Dissolved oxygen dynamics in the hyporheic zone in response to surface flow perturbations. *Water Resources Research*, *53*, 6642–6662. https://doi.org/10.1002/2016WR020296

Kelly, J. F., Bolster, D., Meerschaert, M. M., Drummond, J. D., & Packman, A. I. (2017). FracFit: A robust parameter estimation tool for fractional calculus models. *Water Resources Research*, *53*, 2559–2567. https://doi.org/10.1002/2016WR019748

Kemp, M. J., & Dodds, W. K. (2002). The influence of ammonium, nitrate, and dissolved oxygen concentrations on uptake, nitrification, and denitrification rates associated with prairie stream substrata. *Limnology and Oceanography*, *47*, 1380–1393. https://aslopubs.onlinelibrary.wiley.com/doi/abs/10.4319/lo.2002.47.5.1380

Knapp, J. L. A., & Cirpka, O. A. (2017). Determination of hyporheic travel time distributions and other parameters from concurrent conservative and reactive tracer tests by local-in-global optimization. *Water Resources Research*, *53*, 4984–5001. https://doi.org/10.1002/2017WR020734

Knapp, J. L. A., González-Pinzón, R., Drummond, J. D., Larsen, L. G., Cirpka, O. A., & Harvey, J. W. (2017). Tracer-based characterization of hyporheic exchange and benthic biolayers in streams. *Water Resources Research*, *53*, 1575–1594. https://doi.org/10.1002/2016WR019393

Laloy, E., & Vrugt, J. A. (2012). High-dimensional posterior exploration of hydrologic models using multiple-try DREAM$_{(ZS)}$ and high-performance computing. *Water Resources Research*, *48*, W01526. https://doi.org/10.1029/2011WR010608

Lemke, D., Liao, Z., Wöhling, T., Osenbrück, K., & Cirpka, O. A. (2013). Concurrent conservative and reactive tracer tests in a stream undergoing hyporheic exchange. *Water Resources Research*, *49*, 3024–3037. https://doi.org/10.1002/wrcr.20277

Li, A., Aubeneau, A. F., Bolster, D., Tank, J. L., & Packman, A. I. (2017). Covariation in patterns of turbulence-driven hyporheic flow and denitrification enhances reach-scale nitrogen removal. *Water Resources Research*, *53*, 6927–6944. https://doi.org/10.1002/2016WR019949

Manes, C., Pokrajac, D., McEwan, I., & Nikora, V. (2009). Turbulence structure of open channel flows over permeable and impermeable beds: A comparative study. *Physics of Fluids (1994-present)*, *21*, 125109. http://scitation.aip.org/content/aip/journal/pof2/21/12/10.1063/1.3276292

Margolin, G., Dentz, M., & Berkowitz, B. (2003). Continuous time random walk and multirate mass transfer modeling of sorption. *Chemical physics*, *295*, 71–80.

Mulholland, P. J., Helton, A. M., Poole, G. C., Hall, R. O., Hamilton, S. K., Peterson, B. J., et al. (2008). Stream denitrification across biomes and its response to anthropogenic nitrate loading. *Nature*, *452*, 202–205.

Mulholland, P. J., Tank, J. L., Sanzone, D. M., Wollheim, W. M., Peterson, B. J., Webster, J. R., & Meyer, J. L. (2000). Nitrogen cycling in a forest stream determined by a 15N tracer addition. *Ecological Monographs*, *70*, 471–493. https://doi.org/10.1890/0012-9615(2000)070[0471:NCIAFS]2.0.CO;2

Newbold, J. D., Elwood, J. W., O'Neill, R. V., & Winkle, W. V. (1981). Measuring nutrient spiralling in streams. *Canadian Journal of Fisheries and Aquatic Sciences*, *38*, 860–863. https://doi.org/10.1139/f81-114

Nissan, A., & Berkowitz, B. (2018). Inertial effects on flow and transport in heterogeneous porous media. *Phys. Rev. Lett.*, *120*, 054504. https://link.aps.org/doi/10.1103/PhysRevLett.120.054504

O'Connor, B. L., & Harvey, J. W. (2008). Scaling hyporheic exchange and its influence on biogeochemical reactions in aquatic ecosystems. *Water Resources Research*, *44*, W12423. https://doi.org/10.1029/2008WR007160

O'Connor, B. L., Hondzo, M., & Harvey, J. W. (2010). Predictive modeling of transient storage and nutrient uptake: Implications for stream restoration. *Journal of Hydraulic Engineering*, *136*, 1018–1032. https://ascelibrary.org/doi/abs/10.1061/

Peterson, B. J., Wollheim, W. M., Mulholland, P. J., Webster, J. R., Meyer, J. L., Tank, J. L., et al. (2001). Control of nitrogen export from watersheds by headwater streams. *Science*, *292*, 86–90. 420FU Times Cited:617 Cited References Count:28.

R Core Team (2017). *R: A language and environment for statistical computing*. Vienna, Austria: R Foundation for Statistical Computing. https://www.R-project.org/

Raudenbush, S. W., & Bryk, A. S. (2002). *Hierarchical linear models: Applications and data analysis methods* (2nd ed., Vol. 1). Sage.

Reisinger, A. J., Tank, J. L., & Dee, M. M. (2016). Regional and seasonal variation in nutrient limitation of river biofilms. *Freshwater Science*, *35*, 474–489. https://doi.org/10.1086/685829

Roche, K. R., Drummond, J. D., Boano, F., Packman, A. I., Battin, T. J., & Hunter, W. R. (2017). Benthic biofilm controls on fine particle dynamics in streams. *Water Resources Research*, *53*, 222–236. https://doi.org/10.1002/2016WR019041

Runkel, R. L. (2007). Toward a transport-based analysis of nutrient spiraling and uptake in streams. *Limnology and Oceanography: Methods*, *5*, 50–62.

Schumer, R., Benson, D. A., Meerschaert, M. M., & Baeumer, B. (2003). Fractal mobile/immobile solute transport. *Water Resources Research*, *39*(10), 1296. https://doi.org/10.1029/2003WR002141

Sokolov, I. M., Schmidt, M. G. W., & Sagués, F. (2006). Reaction-subdiffusion equations. *Phys. Rev. E.*, *73*, 031102. https://link.aps.org/doi/10.1103/PhysRevE.73.031102

Stonedahl, S. H., Harvey, J. W., Detty, J., Aubeneau, A., & Packman, A. I. (2012). Physical controls and predictability of stream hyporheic flow evaluated with a multiscale model. *Water Resources Research*, *48*, W10513. https://doi.org/10.1029/2011WR011582

Stream Solute Workshop (1990). Concepts and methods for assessing solute dynamics in stream ecosystems. *Journal of the North American Benthological Society*, *9*, 95–119. http://www.jstor.org/stable/1467445

Tank, J. L., Martí, E., Riis, T., von Schiller, D., Reisinger, A. J., Dodds, W. K., et al. (2018). Partitioning assimilatory nitrogen uptake in streams: An analysis of stable isotope tracer additions across continents. *Ecological Monographs*, *88*, 120–138. https://doi.org/10.1002/ecm.1280

Tank, J. L., Reisinger, A. J., & Rosi, E. J. (2017). *Chapter 31—Nutrient limitation and uptake* (3rd ed., pp. 147–171). Academic Press. https://www.sciencedirect.com/science/article/pii/B9780128130476000097

Tank, J. L., Rosi-Marshall, E. J., Baker, M. A., & Hall, R. O. (2008). Are rivers just big streams? A pulse method to quantify nitrogen demand in a large river. *Ecology*, *89*, 2935–2945.

Tomasek, A. A., Barman, T. D., Wang, P., Kozarek, J. L., Staley, C., Sadowsky, M. J., & Hondzo, M. (2018). The effects of turbulence and carbon amendments on nitrate uptake and microbial gene abundances in stream sediment. *Journal of Geophysical Research: Biogeosciences*, *123*, 1289–1301. https://doi.org/10.1002/2017JG004261

Valett, H. M., Morrice, J. A., Dahm, C. N., & Campana, M. E. (1996). Parent lithology, surface–groundwater exchange, and nitrate retention in headwater streams. *Limnology and oceanography*, *41*, 333–345.

Vitousek, P. M., Aber, J. D., Howarth, R. W., Likens, G. E., Matson, P. A., Schindler, D. W., et al. (1997). Human alteration of the global nitrogen cycle: Sources and consequences. *Ecological Applications*, *7*, 737–750. https://doi.org/10.1890/1051-0761(1997)007[0737:HAOTGN]2.0.CO;2

Voermans, J. J., Ghisalberti, M., & Ivey, G. N. (2018). A model for mass transport across the sediment-water interface. *Water Resources Research*, *54*, 2799–2812. https://doi.org/10.1002/2017WR022418

Vrugt, J. A. (2016). Markov chain Monte Carlo simulation using the DREAM software package: Theory, concepts, and MATLAB implementation. *Environmental Modelling & Software*, *75*, 273–316. http://www.sciencedirect.com/science/article/pii/S1364815215300396

Webster, J. R., & Patten, B. C. (1979). Effects of watershed perturbation on stream potassium and calcium dynamics. *Ecological monographs*, *49*, 51–72.

Zarnetske, J. P., Gooseff, M. N., Brosten, T. R., Bradford, J. H., McNamara, J. P., & Bowden, W. B. (2007). Transient storage as a function of geomorphology, discharge, and permafrost active layer conditions in Arctic tundra streams. *Water Resources Research*, *43*, W07410. https://doi.org/10.1029/2005WR004816

Zarnetske, J. P., Haggerty, R., & Wondzell, S. M. (2015). Coupling multiscale observations to evaluate hyporheic nitrate removal at the reach scale. *Freshwater Science*, *34*, 172–186.

Zarnetske, J. P., Haggerty, R., Wondzell, S. M., & Baker, M. A. (2011). Dynamics of nitrate production and removal as a function of residence time in the hyporheic zone. *Journal of Geophysical Research*, *116*, G01025. https://doi.org/10.1029/2010JG001356